




# An unconditionally stable splitting method for the Allen–Cahn equation with logarithmic free energy

Jintae Park · Chaeyoung Lee · Yongho Choi ·  
Hyun Geun Lee · Soobin Kwak ·  
Youngjin Hwang · Junseok Kim 

Received: 13 June 2021 / Accepted: 4 December 2021 / Published online: 10 January 2022  
© The Author(s), under exclusive licence to Springer Nature B.V. 2022

**Abstract** We present an unconditionally stable splitting method for the Allen–Cahn (AC) equation with logarithmic free energy which is more physically meaningful than the commonly used polynomial potentials. However, owing to the singularity of the logarithmic free energy, it is difficult to develop unconditionally stable computational methods for the AC equation with logarithmic potential. To overcome this difficulty, prior works added a stabilizing term to the logarithmic energy or used a regularized potential. In this study, the AC equation with logarithmic potential is solved by using an operator splitting method without adding a stabilizing term nor regularizing the logarithmic energy. The equation involving logarithmic free energy potential is solved using an interpolation method; the other diffusion equation is solved numerically by applying a finite difference method. Each solution algorithm is unconditionally stable, the proposed scheme is unconditionally stable. Various computational experiments demonstrate the performance of the proposed method.

**Keywords** Allen–Cahn equation · Flory–Huggins potential · Unconditionally stable scheme

---

J. Park · C. Lee · S. Kwak · Y. Hwang · J. Kim (✉)  
Department of Mathematics, Korea University, Seoul 02841, Republic of Korea  
e-mail: cfdkim@korea.ac.kr

J. Park  
e-mail: jintae2002@korea.ac.kr

C. Lee  
e-mail: chael1228@korea.ac.kr

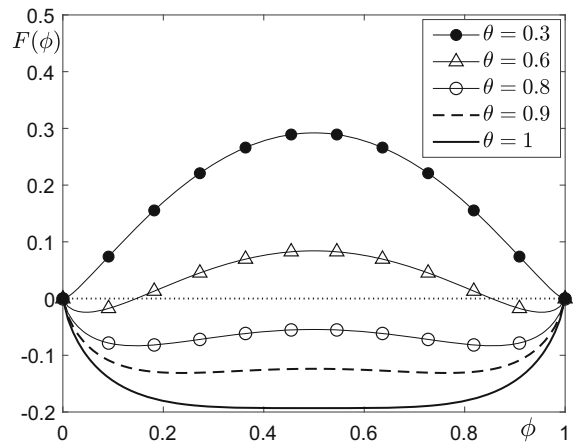
S. Kwak  
e-mail: soobin23@korea.ac.kr

Y. Hwang  
e-mail: youngjin\_hwang@korea.ac.kr

Y. Choi  
Department of Mathematics and Big Data, Daegu University, Gyeongsan-si, Gyeongsangbuk-do 38453, Republic of Korea  
e-mail: yongho\_choi@daegu.ac.kr

H. G. Lee  
Department of Mathematics, Kwangwoon University, Seoul 01897, Republic of Korea  
e-mail: leeh1@kw.ac.kr

**Fig. 1** Flory–Huggins energy potential functions,  $F(\phi) = \theta[\phi \ln(\phi) + (1 - \phi) \ln(1 - \phi)] + 2\theta_c \phi(1 - \phi)$ , for  $0 < \phi < 1$ ,  $\theta_c = 1$ , and  $\theta = 0.3, 0.6, 0.8, 0.9$ , and 1



### 1 Introduction

We consider an unconditionally stable numerical method for the Allen–Cahn (AC) equation [1]:

$$\frac{\partial \phi(\mathbf{x}, t)}{\partial t} = -F'(\phi(\mathbf{x}, t)) + \epsilon^2 \Delta \phi(\mathbf{x}, t), \quad \mathbf{x} \in \Omega, \quad t > 0, \tag{1}$$

where  $\phi(\mathbf{x}, t)$  is the phase field in the domain  $\Omega \subset \mathbb{R}^d$  ( $d = 1, 2, 3$ ) and  $\epsilon$  is a small positive constant value. Let

$$\mathcal{E}(\phi) = \int_{\Omega} \left( F(\phi) + \frac{\epsilon^2}{2} |\nabla \phi|^2 \right) d\mathbf{x}. \tag{2}$$

Equation (1) can be obtained from Eq. (2) in an  $L^2$ -gradient flow. From Eq. (2), we can then obtain

$$\frac{d}{dt} \mathcal{E}(\phi) = \int_{\Omega} \left( \frac{\partial \phi}{\partial t} F'(\phi) + \epsilon^2 \nabla \frac{\partial \phi}{\partial t} \cdot \nabla \phi \right) d\mathbf{x} = \int_{\Omega} \phi_t (F'(\phi) - \epsilon^2 \Delta \phi) d\mathbf{x} = - \int_{\Omega} (\phi_t)^2 d\mathbf{x} \leq 0, \tag{3}$$

which implies that the total energy decreases over time. Here, we used the zero Neumann boundary condition. The logarithmic energy potential is defined as

$$F(\phi) = \theta[\phi \ln(\phi) + (1 - \phi) \ln(1 - \phi)] + 2\theta_c \phi(1 - \phi), \quad \text{for } 0 < \phi < 1, \tag{4}$$

where  $\theta$  and  $\theta_c$  are the absolute and critical temperatures, respectively [2]. For a detailed derivation of Eq. (4), see the review paper [3]. For the sake of simplicity, we assume that  $\theta_c = 1$  in this paper. Figure 1 shows  $F(\phi)$  with different  $\theta$  values.

The AC equation with logarithmic free energy is more physically meaningful than the commonly used fourth-order polynomial potential. However, owing to the singularity of the logarithmic free energy (4) at  $\phi = 0$  and 1, it is difficult to develop unconditionally stable computational schemes for the AC equation with logarithmic potential. To overcome this difficulty, either a stabilizing term is added to the logarithmic energy [4] or a regularized potential is used [5]. The authors in [6] studied a maximum principle preserving scheme for a generalized AC equation. Bartels and Müller [7] investigated the dynamics of the AC equation with logarithmic potentials. In [8], numerical methods solving the Cahn–Hilliard equation with the Flory–Huggins energy potential were analyzed and studied. In this study, we numerically solve the AC equation with logarithmic potential without adding a stabilizing term nor regularizing the logarithmic energy.

The contents of this article are as follows. In Sect. 2, the proposed computational scheme is presented for the AC equation with the Flory–Huggins potential. In Sect. 3, we present the results of computational experiments conducted to verify the robustness of the proposed scheme. Conclusions are given in Sect. 4.

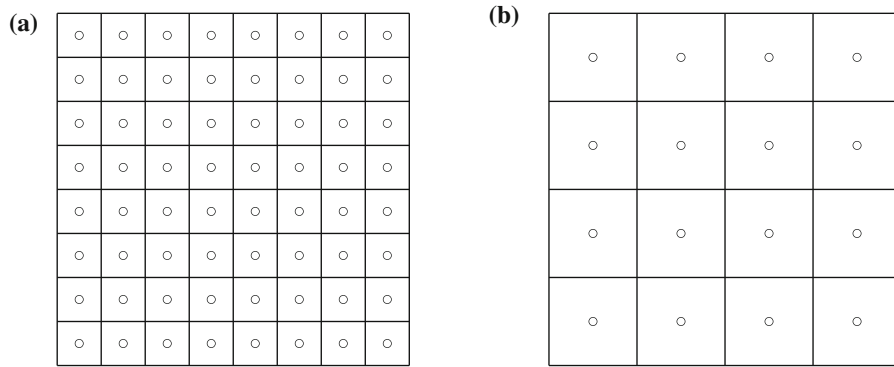


**Fig. 2** Grids with spatial step sizes: **a**  $h$  and **b**  $2h$

### 2 Governing equation and numerical solution

The governing equation with the logarithmic potential energy is as follows:

$$\frac{\partial \phi(\mathbf{x}, t)}{\partial t} = -\theta[\ln(\phi(\mathbf{x}, t)) - \ln(1 - \phi(\mathbf{x}, t))] - 2(1 - 2\phi(\mathbf{x}, t)) + \epsilon^2 \Delta \phi(\mathbf{x}, t). \tag{5}$$

To efficiently solve Eq. (5), we apply a recently developed interpolation method [9]. Specifically, for the second-order operator splitting method [10], we divide Eq. (5) into two parts, linear and nonlinear operators, and then numerically solve the governing equation through the following three steps:

$$\phi(\mathbf{x}, t + \Delta t) = \left( \mathcal{L}^{\Delta t/2} \circ \mathcal{N}^{\Delta t} \circ \mathcal{L}^{\Delta t/2} \right) \phi(\mathbf{x}, t) + \mathcal{O}(\Delta t^3), \tag{6}$$

where  $\mathcal{L}^{\Delta t}$  and  $\mathcal{N}^{\Delta t}$  are linear and nonlinear operators with time step size  $\Delta t$ , respectively. The linear operator is defined as  $\mathcal{L}^{\Delta t} \phi(\mathbf{x}, t) = \phi(\mathbf{x}, t + \Delta t)$ , where  $\phi(\mathbf{x}, t + \Delta t)$  is a solution to  $\partial \phi(\mathbf{x}, t) / \partial t = \epsilon^2 \Delta \phi(\mathbf{x}, t)$ . The nonlinear operator is defined as  $\mathcal{N}^{\Delta t} \phi(\mathbf{x}, t) = \phi(\mathbf{x}, t + \Delta t)$ , where  $\phi(\mathbf{x}, t + \Delta t)$  is a solution of  $\partial \phi(\mathbf{x}, t) / \partial t = -\theta[\ln(\phi(\mathbf{x}, t)) - \ln(1 - \phi(\mathbf{x}, t))] - 2(1 - 2\phi(\mathbf{x}, t))$ . If two operators  $\mathcal{L}^{\Delta t}$  and  $\mathcal{N}^{\Delta t}$  have at least second-order accuracy with respect to time, the numerical scheme using Eq. (6) is theoretically guaranteed to have second-order accuracy with respect to time [11, 12]. Now, we present the proposed numerical scheme for the AC equation with the Flory–Huggins potential energy in a two-dimensional space  $\Omega = (L_x, R_x) \times (L_y, R_y)$ . Let  $N_x$  and  $N_y$  be even integers and  $h = (R_x - L_x) / N_x = (R_y - L_y) / N_y$  be a uniform spatial step size. In addition, let  $\phi_{mn}^k$  be a numerical approximation of  $\phi(x_m, y_n, t_k)$ , where  $x_m = L_x + (m - 0.5)h$ ,  $y_n = L_y + (n - 0.5)h$ , and  $t_k = k \Delta t$ . First, we solve the linear equation

$$\frac{\partial \phi(\mathbf{x}, t)}{\partial t} = \epsilon^2 \Delta \phi(\mathbf{x}, t) \tag{7}$$

using the Crank–Nicolson (CN) scheme [13]. That is, we solve Eq. (8) using a multigrid method.

$$\frac{\phi_{mn}^{k+\frac{1}{2}} - \phi_{mn}^k}{\Delta t} = \frac{\epsilon^2}{2} \left( \Delta_h \phi_{mn}^k + \Delta_h \phi_{mn}^{k+\frac{1}{2}} \right), \tag{8}$$

where  $\Delta_h \phi_{mn} = (\phi_{m+1,n} + \phi_{m-1,n} + \phi_{m,n+1} + \phi_{m,n-1} - 4\phi_{mn}) / h^2$ . For completeness of the exposition, we provide a brief description of the multigrid method used for the pressure field in the Navier–Stokes equation [14]. To describe the multigrid procedure, let us consider a small discrete domain  $\Omega_h$  ( $8 \times 8$  grid) for Eq. (8) (see Fig. 2a).

Equation (8) can be expressed as

$$L(\phi_{h,mn}^{k+\frac{1}{2}}) = f_{h,mn} \quad \text{on } \Omega_h, \tag{9}$$

where the subscript  $h$  indicates the discrete values on  $\Omega_h$ ,

$$L(\phi_{h,mn}^{k+\frac{1}{2}}) = \frac{\phi_{h,mn}^{k+\frac{1}{2}}}{\Delta t} - \frac{\epsilon^2}{2} \Delta_h \phi_{h,mn}^{k+\frac{1}{2}}, \quad \text{and} \quad f_{h,mn} = \frac{\phi_{h,mn}^k}{\Delta t} + \frac{\epsilon^2}{2} \Delta_h \phi_{h,mn}^k.$$

We define a multigrid cycle as follows:

$$\phi_h^{k+\frac{1}{2},p+1} = \text{MGcycle}(\phi_h^{k+\frac{1}{2},p}, f_h, \nu),$$

where  $\phi_h^{k+\frac{1}{2},p+1}$  and  $\phi_h^{k+\frac{1}{2},p}$  are the approximations of  $\phi_h^{k+\frac{1}{2}}$  before and after one multigrid cycle, respectively; in addition,  $\nu$  is the number of smoothing relaxations. We use a Gauss–Seidel relaxation operator in the multigrid method. First, we rewrite Eq. (9) as

$$\phi_{h,mn}^{k+\frac{1}{2}} = \left[ f_{h,mn} + \epsilon^2 \frac{\phi_{h,m-1,n}^{k+\frac{1}{2}} + \phi_{h,m+1,n}^{k+\frac{1}{2}} + \phi_{h,m,n-1}^{k+\frac{1}{2}} + \phi_{h,m,n+1}^{k+\frac{1}{2}}}{2h^2} \right] / \left( \frac{1}{\Delta t} + \frac{2\epsilon^2}{h^2} \right). \tag{10}$$

Next, we apply the Gauss–Seidel update ordering to Eq. (10) as

$$\bar{\phi}_{h,mn}^{k+\frac{1}{2},p} = \left[ f_{h,mn} + \epsilon^2 \frac{\bar{\phi}_{h,m-1,n}^{k+\frac{1}{2},p} + \phi_{h,m+1,n}^{k+\frac{1}{2},p} + \bar{\phi}_{h,m,n-1}^{k+\frac{1}{2},p} + \phi_{h,m,n+1}^{k+\frac{1}{2},p}}{2h^2} \right] / \left( \frac{1}{\Delta t} + \frac{2\epsilon^2}{h^2} \right),$$

where  $\bar{\phi}_{h,mn}^{k+\frac{1}{2},p}$  denotes the updated value after taking the  $p$ th Gauss–Seidel iteration. In the multigrid cycle, we first apply a pre-smoothing step as follows:

$$\bar{\phi}_h^{k+\frac{1}{2},\nu} = \text{SMOOTH}(\phi_h^{k+\frac{1}{2},0}, f_h),$$

which means taking  $\nu$  relaxation steps with the initial guess  $\phi_h^{k+\frac{1}{2},0}$  and the source term  $f_h$  to obtain the approximation  $\bar{\phi}_h^{k+\frac{1}{2},\nu}$ . Next, we compute the defect as  $\bar{d}_h^\nu = f_h - L(\bar{\phi}_h^{k+\frac{1}{2},\nu})$ , and restrict it as  $\bar{d}_{2h}^\nu = I_h^{2h} \bar{d}_h^\nu$ . We then solve the following equation:

$$L(\psi_{2h}) = \bar{d}_{2h}^\nu \quad \text{on } \Omega_{2h},$$

where  $\Omega_{2h}$  is the coarse grid, as shown in Fig. 2b. We interpolate the coarse grid correction as  $\psi_h = I_{k-1}^k \psi_{2h}$  and compute the corrected solution on  $\Omega_h$  as

$$\phi_h^{k+\frac{1}{2},\nu, \text{ after CGC}} = \bar{\phi}_h^{k+\frac{1}{2},\nu} + \psi_h.$$

Finally, we take a post-smoothing step:

$$\phi_h^{k+\frac{1}{2},p+1} = \text{SMOOTH}(\phi_h^{k+\frac{1}{2},\nu, \text{ after CGC}}, f_h).$$

These steps consist of a two-grid correction scheme. The multigrid procedure is defined as the recursively applied two-grid correction schemes. This is a multigrid cycle, which terminates if the consequence error  $\|\phi_h^{k+\frac{1}{2},p+1} - \phi_h^{k+\frac{1}{2},p}\|_\infty$  is smaller than a given tolerance, where

$$\|\phi\|_\infty = \max_{1 \leq m \leq N_x, 1 \leq n \leq N_y} |\phi_{mn}|.$$

More details on the multigrid procedure can be found in [14].

Next, we solve the following nonlinear equation:

$$\frac{\partial \phi(\mathbf{x}, t)}{\partial t} = -F'(\phi(\mathbf{x}, t)) = -\theta[\ln(\phi(\mathbf{x}, t)) - \ln(1 - \phi(\mathbf{x}, t))] - 2(1 - 2\phi(\mathbf{x}, t)). \tag{11}$$

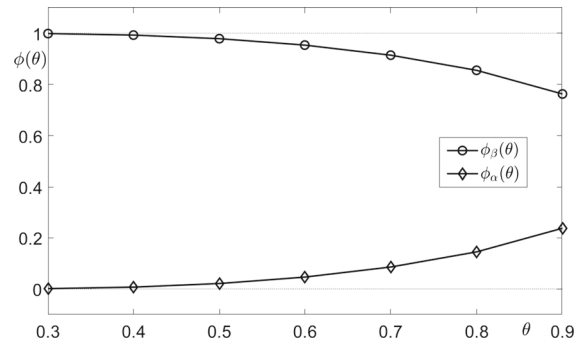
However, unlike the fourth-order polynomial free energy potential, there is no closed-form solution for the logarithmic free energy potential. To stably solve Eq. (11), we propose the following algorithm based on the recently developed interpolation method [9]. Let  $\phi_\alpha$  and  $\phi_\beta$  be the two critical values of  $F(\phi)$ , that is,  $F'(\phi_\alpha) = F'(\phi_\beta) = 0$ . Because of the symmetrical feature of  $F(\phi)$ ,  $\phi_\alpha + \phi_\beta = 1$  is satisfied. To obtain  $\phi_\alpha$ , Newton’s method [15] is used. Using three different tolerances,  $\text{tol} = 1\text{e}-4, 1\text{e}-8, \text{ and } 1\text{e}-12$ , we compute  $\phi_\alpha$  and the number of iterations for each tolerance. The initial guess is set to  $\phi_0 = 0.999$  and we conduct the iterative process  $\phi_{k+1} = \phi_k - F'(\phi_k)/F''(\phi_k)$

**Table 1** For each tolerance, the values of  $\phi_\alpha$  are given with respect to  $\theta = 0.3, 0.4, 0.5, 0.6, 0.7, 0.8,$  and  $0.9$

Tol	$\theta$						
	0.3	0.4	0.5	0.6	0.7	0.8	0.9
1e-4	0.00129(4)	0.00715(5)	0.02122(6)	0.04633(7)	0.08568(8)	0.14476(8)	0.23725(9)
1e-8	0.00129(5)	0.00718(7)	0.02124(8)	0.04633(8)	0.08568(9)	0.14479(9)	0.23729(10)
1e-12	0.00129(6)	0.00718(7)	0.02124(8)	0.04633(9)	0.08568(9)	0.14479(10)	0.23729(11)

The number of iterations are shown in parentheses. Notably,  $\phi_\beta = 1 - \phi_\alpha$

**Fig. 3** Values of  $\phi_\alpha$  and  $\phi_\beta$  with respect to  $\theta$



until  $|F'(\phi_k)/F''(\phi_k)| < tol$ . Then, we set  $\phi_\alpha = \phi_{k+1}$ . Table 1 shows  $\phi_\alpha$  and the number of iterations with various values of  $\theta$  and  $tol$ . In this case, the value of  $\phi_\beta$  can be obtained using the condition  $\phi_\alpha + \phi_\beta = 1$ .

From now on, we will use  $tol = 1e-12$  for all numerical experiments. Figure 3 shows the values of  $\phi_\alpha$  and  $\phi_\beta$  with respect to  $\theta$ .

Let us assume  $\theta, \epsilon,$  and  $\Delta t$  are given. We uniformly discretize the interval  $[\phi_\alpha, \phi_\beta] \subset [0, 1]$ , that is,  $I = \{I_i | I_i = \phi_\alpha + (\phi_\beta - \phi_\alpha)(i - 1)/(M - 1), \text{ for } i = 1, \dots, M\}$ , where  $M$  is an odd integer and  $I$  always includes 0.5. We solve Eq. (11) on  $I$  with  $\Delta\tau = \Delta t/N_\tau$  until  $t = \Delta t$ . Note that  $N_\tau$  is defined below. Figure 4 displays the computational results of Eq. (11) on  $I$  at  $t = \Delta t$  using the Euler method with  $\Delta\tau$  and the initial condition,  $\Phi_i(0) = I_i$  for  $i = 1, \dots, M$ . That is,

$$\Phi_i((s + 1)\Delta\tau) = \Phi_i(s\Delta\tau) - \Delta\tau F'(\Phi_i(s\Delta\tau)), \text{ for } s = 0, \dots, N_\tau - 1. \tag{12}$$

After computing all  $\Phi_i(\Delta t)$  for  $i = 1, \dots, M$  once, we use these values to solve Eq. (11) by using an interpolation.

Next, we compute  $N_\tau$  to stably evaluate Eq. (12) for the given values of  $\theta, \epsilon,$  and  $\Delta t$ . If  $I_i = \phi_\alpha, 0.5,$  or  $\phi_\beta$ , then from Eq. (12) we have

$$\Phi_i((s + 1)\Delta\tau) = I_i, \text{ for } s = 0, \dots, N_\tau - 1. \tag{13}$$

Next, let us suppose  $0.5 < I_i < \phi_\beta$  and  $\Phi_i(0) = I_i$ . Then from Eq. (12) we have

$$\Phi_i(\Delta\tau) = I_i - \Delta\tau F'(I_i). \tag{14}$$

As can be seen in Fig. 5,  $F'(I_i) = \theta \ln \frac{I_i}{1-I_i} + 2(1 - 2I_i) < 0$  for  $0.5 < I_i < \phi_\beta$  and  $\theta < 1$ ; therefore, we have  $\Phi_i(\Delta\tau) > 0.5$  from Eq. (14) for any  $\Delta\tau$ .

In addition, we want to find  $\Delta\tau$  satisfying the condition  $I_i - \Delta\tau F'(I_i) < \phi_\beta$ , that is,

$$\Delta\tau < \frac{I_i - \phi_\beta}{F'(I_i)} = \frac{I_i - \phi_\beta}{\theta \left[ \ln \left( \frac{I_i}{1-I_i} \right) \right] + 2(1 - 2I_i)}. \tag{15}$$

The term on the right-hand side of inequality (15) decreases with respect to  $I_i$ , as shown in Fig. 6.

Therefore, we consider the limit of the term as  $I_i$  approaches  $\phi_\beta$ . By using L'Hôpital's rule, we have

$$\Delta\tau \leq \lim_{I_i \rightarrow \phi_\beta} \frac{I_i - \phi_\beta}{\theta \left[ \ln \left( \frac{I_i}{1-I_i} \right) \right] + 2(1 - 2I_i)} = \lim_{I_i \rightarrow \phi_\beta} \frac{1}{\theta \left( \frac{1}{I_i} + \frac{1}{1-I_i} \right) - 4} = \frac{1}{\theta \left( \frac{1}{\phi_\beta} + \frac{1}{1-\phi_\beta} \right) - 4}. \tag{16}$$

**Fig. 4** Numerical solution  $\Phi(\Delta t)$  of Eq. (11) on  $I$

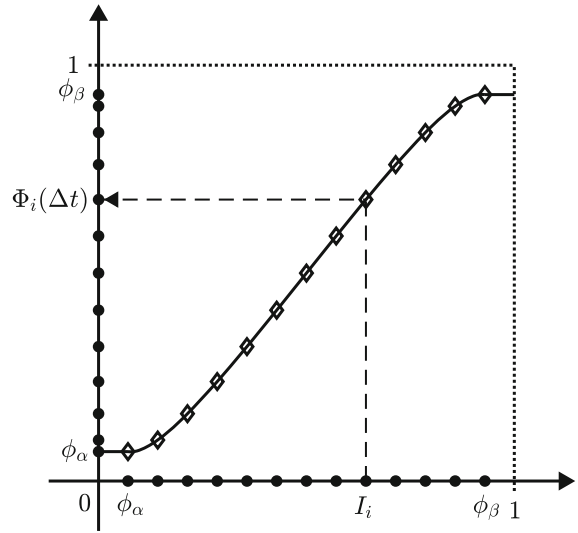


**Fig. 5**  $F'(I_i) = \theta[\ln(I_i) - \ln(1 - I_i)] + 2(1 - 2I_i)$  for  $\theta = 0.3, 0.6, 0.8, 0.9,$  and  $1$ . Blue lines indicate the value of  $\phi_\beta$  and have the same symbols for each  $\theta$ . (Color figure online)

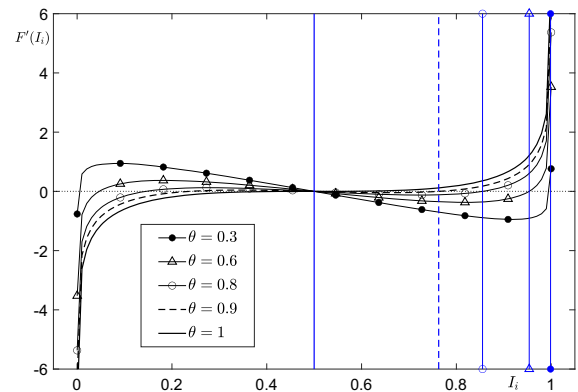


**Fig. 6** Semilogy plot of  $(I_i - \phi_\beta)/F'(I_i)$  with respect to  $I_i$ . Here,  $\theta = 0.8$  is used

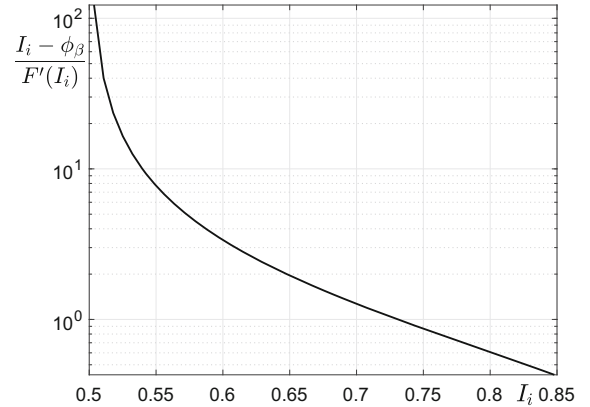
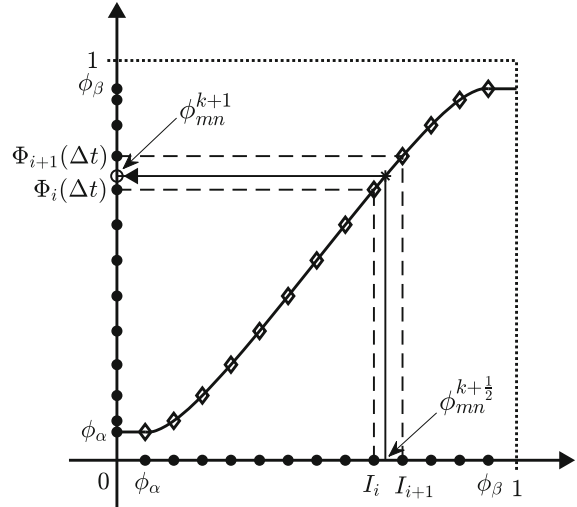


**Table 2** Least upper bound of  $\Delta\tau$  with different values of  $\theta$

$\theta$	0.3	0.4	0.5	0.6	0.7	0.8	0.9
$\Delta\tau$	0.0044	0.0192	0.0499	0.1044	0.2026	0.4064	1.0279

**Fig. 7** Schematic diagram of the interpolation



Using the result in Eq. (16), Table 2 lists the least upper bound of  $\Delta\tau$  with different values of  $\theta$ .

From the definition of  $\Delta\tau = \Delta t/N_\tau$  and the stability condition (16),  $N_\tau \geq \Delta t \left( \theta \left( \frac{1}{\phi_\beta} + \frac{1}{1-\phi_\beta} \right) - 4 \right)$  should be satisfied. Therefore, unless otherwise specified, we set  $N_\tau = \left\lceil \Delta t \left( \theta \left( \frac{1}{\phi_\beta} + \frac{1}{1-\phi_\beta} \right) - 4 \right) \right\rceil + 1$ , where  $\lceil x \rceil$  is the greatest integer less than or equal to  $x$ . Given the intermediate solution from the first step,  $\phi_{mn}^{k+1/2}$ , the second step is to solve Eq. (11) by using the pre-computed values and interpolation. We can find a node  $I_i$  satisfying  $I_i \leq \phi_{mn}^{k+1/2} \leq I_{i+1}$  for some  $i$  and  $1 \leq i \leq M - 1$ . We then define

$$\phi_{mn}^{k+1} = \frac{I_{i+1} - \phi_{mn}^{k+1/2}}{I_{i+1} - I_i} \Phi_i(\Delta t) + \frac{\phi_{mn}^{k+1/2} - I_i}{I_{i+1} - I_i} \Phi_{i+1}(\Delta t), \tag{17}$$

as schematically illustrated in Fig. 7.

The proposed numerical scheme is unconditionally stable because each step in the operator splitting method is also unconditionally stable.

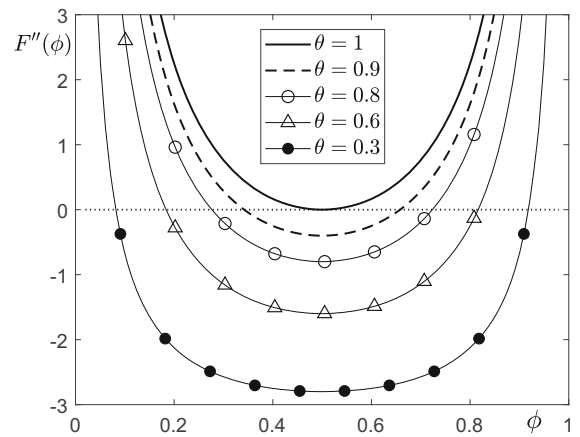
### 3 Computational tests

We perform several computational tests to show the dynamics of the AC equation with logarithmic free energy potential. Unless otherwise stated, we use  $M = 101$ . Notably, we should have an interval for  $\phi$  satisfying  $F''(\phi) < 0$  to obtain a double-well potential. Figure 8 shows  $F''(\phi) = \theta[1/\phi + 1/(1 - \phi)] - 4$  with various  $\theta$  values. To find the condition for  $\theta$ , let us consider the following equation:

$$F''(\phi) = \theta \left( \frac{1}{\phi} + \frac{1}{1 - \phi} \right) - 4 = \frac{\theta}{\phi(1 - \phi)} - 4 \geq 4\theta - 4, \tag{18}$$

which implies  $F''(\phi) \geq 0$  if  $\theta \geq 1$ . Therefore, to have a double-well potential,  $\theta$  should be less than 1.

**Fig. 8** Plot of  $F''(\phi) = \theta[1/\phi + 1/(1 - \phi)] - 4$  with  $\theta = 0.3, 0.6, 0.8, 0.9,$  and 1



### 3.1 Maximum principle

We demonstrate that our proposed method preserves the maximum principle, which is essential for the logarithmic energy potential. The discrete governing equation can be divided into two parts: linear and nonlinear operators, as indicated in Eq. (6). In the first step, the CN scheme (8) is unconditionally stable from the von Neumann analysis [16, 17]. The second step is unconditionally stable because of the definition of the subcycling update of the time step, as described in the inequality (15), and the interpolation with the outside cut-off in interval  $[\phi_\alpha, \phi_\beta]$ . Therefore, the overall proposed scheme is unconditionally stable. Furthermore, we can theoretically guarantee the maximum principle for both the nonlinear and linear equations if the initial condition is in the interval  $[\phi_\alpha, \phi_\beta]$ . Now, we verify the maximum principle through a numerical test. Let  $\phi(x, 0) = (\phi_\beta - \phi_\alpha) \text{rand}(x) + \phi_\alpha$  be the initial condition on  $\Omega = (0, 1)$ , where  $\text{rand}(x)$  is a random number between 0 and 1. The numerical tests are conducted with two different  $\theta$  values while  $N_x = 128$ ,  $h = 1/N_x$ ,  $\Delta t = 0.001$ , and  $\epsilon = 0.02$  are fixed. Herein, we take  $\theta = 0.3$  and  $\theta = 0.9$ . As observed earlier,  $\phi_\alpha$  and  $\phi_\beta$  have different values depending on  $\theta$ ; it can also be verified that the maximum principle is preserved as shown in Fig. 9a and c. Figure 9b and d shows the temporal evolution of the maximum and minimum values of  $\phi(x, t)$  over time, which also suggests that the values do not go beyond the range  $[\phi_\alpha, \phi_\beta]$ .

### 3.2 Unconditional stability

To show the unconditional stability of the proposed method, let us consider the scheme used, i.e.,

$$\phi(\mathbf{x}, t + \Delta t) = \left( \mathcal{L}^{\Delta t/2} \circ \mathcal{N}^{\Delta t} \circ \mathcal{L}^{\Delta t/2} \right) \phi(\mathbf{x}, t),$$

where  $\mathcal{L}^{\Delta t}$  and  $\mathcal{N}^{\Delta t}$  are the linear and nonlinear operators with the time step size  $\Delta t$ , respectively. The proposed method consists of the following two steps:

- Step 1: The heat equation is solved using the CN scheme, which is unconditionally stable. This can be proved from the von Neumann analysis [16, 17].
- Step 2: The nonlinear equation is solved using the explicit Euler scheme and the interpolation method. This method also guarantees an unconditional stability owing to the definition of a subcycling update of the time step and interpolation.

Therefore, because both steps have unconditional stability, the entire method guarantees the unconditional stability. Now, numerical tests are conducted to verify that our proposed method is unconditionally stable. On a one-dimensional domain  $\Omega = (0, 1)$ , the initial condition is  $\phi(x, 0) = 0.5 + 0.1(\text{rand}(x) - 0.5)$ . The parameters



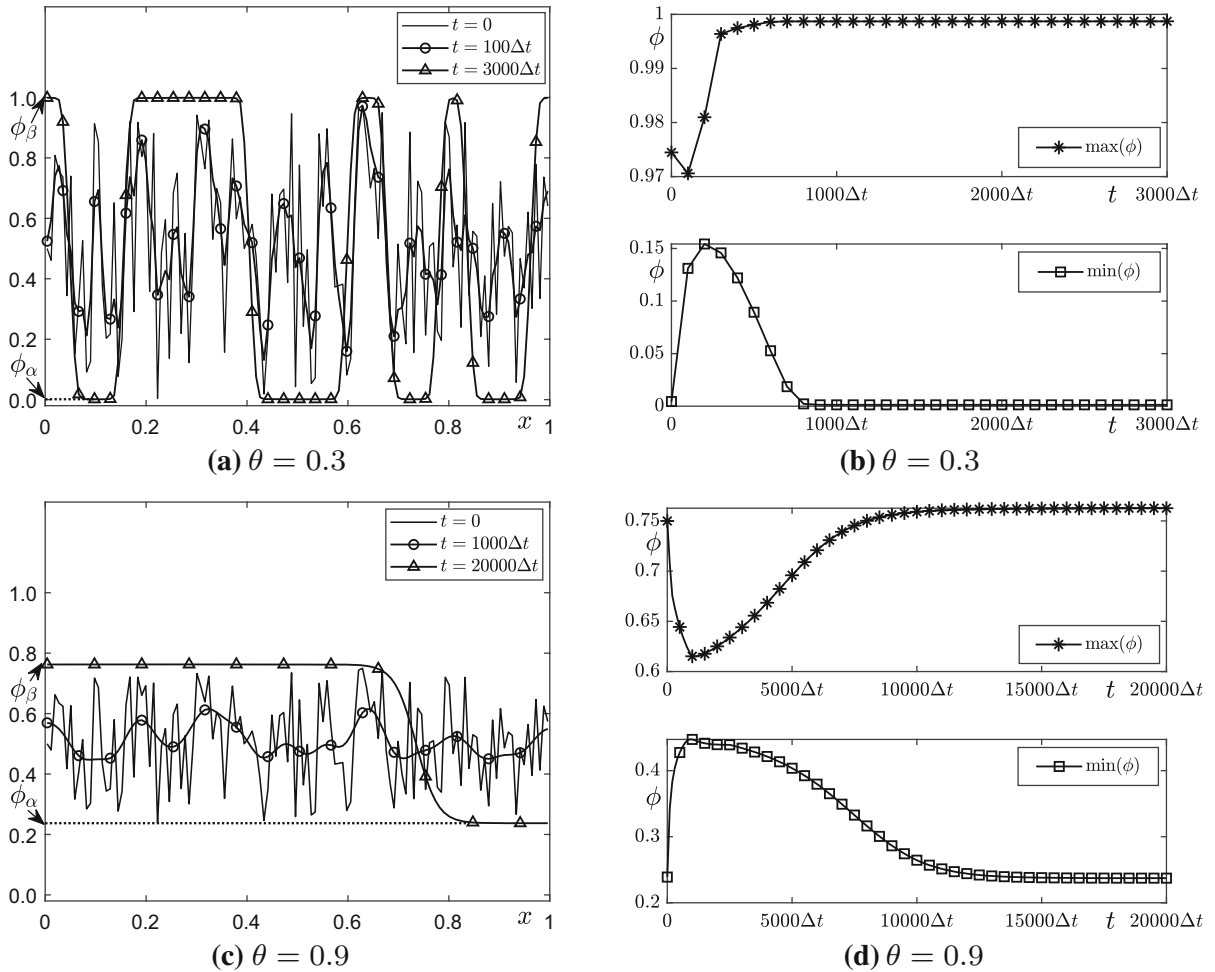


**Fig. 9** Snapshots of temporal evolution of the random initial concentration  $(\phi_\beta - \phi_\alpha)\text{rand}(x) + \phi_\alpha$  at different times with **a**  $\theta = 0.3$  and **c**  $\theta = 0.9$ . For each  $\theta$ , **b** and **d** show the temporal evolutions of the maximum (top) and minimum (bottom) of  $\phi(x, t)$  over time

are  $N_x = 128$ ,  $h = 1/N_x$ ,  $\theta = 0.8$ , and  $\epsilon = 0.02$ . We use three different time steps  $\Delta t = h^2$ ,  $10h^2$ , and  $100h^2$  with a fixed final time of  $T = 10000h^2$ . As shown in Fig. 10, even if the temporal step size becomes large, the numerical solutions do not blow up and show stable results.

### 3.3 Convergence and computational cost tests

A convergence test is conducted to investigate the accuracy of the proposed method, which is theoretically second-order accuracy in both space and time. Therefore, we compute the accuracy of the numerical scheme by concurrently decreasing both the spatial and temporal step sizes by half. On the domain  $\Omega = (0, 1)$ , the initial condition is set to  $\phi(x, 0) = 0.5 + 0.3 \cos(2\pi x)$ . The parameters  $\theta = 0.8$ ,  $\epsilon = 0.02$ , and the final time  $T = 0.025/64$  are fixed. The spatial step size is  $h = 1/N_x$ , and the temporal step size is  $\Delta t = T/N_t$ , where  $N_x$  and  $N_t$  are positive integers. The error is defined as  $e_{N_x}^{N_t} = \phi_{N_x}^{N_t} - \frac{1}{2}(\phi_{2N_x 2t}^{2N_t} + \phi_{2N_x 2t}^{2N_t})$  and the rate of convergence is defined as the ratio of successive  $l_2$ -norm errors as  $\log_2(\|e_{N_x}^{N_t}\|_2 / \|e_{2N_x}^{2N_t}\|_2)$ . Table 3 lists the  $l_2$ -errors and rates of convergence of the

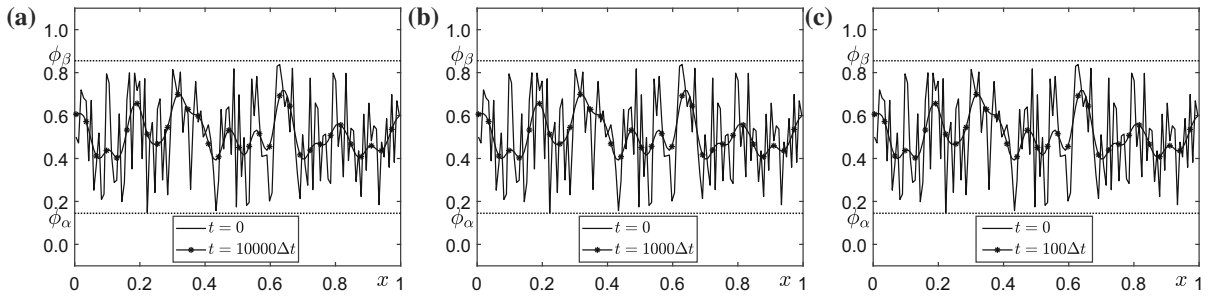
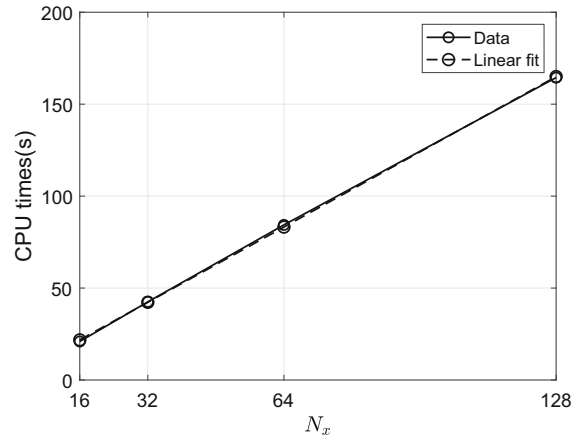


**Fig. 10** Snapshots at final time of  $T = 10,000h^2$  with the random initial concentration  $\phi(x, 0)$ . Three different time steps are used: **a**  $\Delta t = h^2$ , **b**  $\Delta t = 10h^2$ , and **c**  $\Delta t = 100h^2$

**Table 3**  $l_2$ -errors and rates of convergence with respect to spatial and temporal step sizes

$N_x \times N_t$	$64 \times 25$	Rate	$128 \times 50$	Rate	$256 \times 100$	Rate	$512 \times 200$
	$128 \times 50$		$256 \times 100$		$512 \times 200$		$1024 \times 400$
$l_2$ error	$6.4038e-5$	2.00	$1.5987e-5$	2.00	$4.0052e-6$	2.00	$9.9967e-7$

**Fig. 11** CPU time according to various spatial step sizes



proposed method with respect to spatial and temporal step sizes and shows that the proposed scheme is second-order accuracy in both space and time.

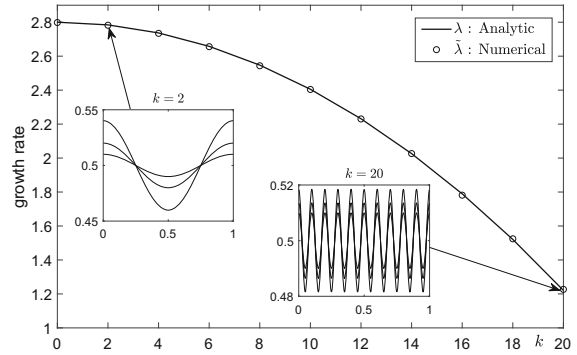
Next, we measure the CPU time (seconds) with respect to the spatial step size. Note that this experiment is calculated using MATLAB R2020b software on an Intel Core i5-6400 CPU machine at 2.71GHz with 4 GB of memory. The parameters  $\Delta t = 1/128^2$  and  $N_t = 10^6$  are used, and the other conditions are the same as those applied in the above test. For  $N_x = 16, 32, 64,$  and  $128$ , the CPU time is measured as 20.952, 42.499, 84.344, and 164.468. As shown in Fig. 11, we can observe the linear fitting for the CPU times, which implies the complexity of the algorithm follows  $O(N_x)$ .

### 3.4 Linear stability analysis

We investigate the linear stability of the governing equation around  $\phi \equiv 0.5$ . Linearizing the AC equation (5) with the logarithmic free energy potential about  $\phi \equiv 0.5$  yields

$$\phi_t = -(4\theta - 4)(\phi - 0.5) + \epsilon^2 \Delta \phi.$$

**Fig. 12** Growth rates of analytic and numerical solutions for different even wave numbers  $k$  ( $k = 0, 2, 4, \dots, 20$ ). The small inset figures show temporal evolutions of the numerical solution for  $k = 2$  and  $k = 20$



We assume the solution to have the following form:

$$\phi(x, t) = 0.5 + \alpha(t) \cos(k\pi x), \tag{19}$$

where  $\alpha(t)$  is an amplitude at wave numbers  $k$  satisfying  $|\alpha(0)| \ll 1$ . Substituting Eq. (19) into the linearized equation, we then obtain

$$\alpha'(t) = [4 - 4\theta - \epsilon^2 \pi^2 k^2] \alpha(t). \tag{20}$$

The solution to Eq. (20) is  $\alpha(t) = \alpha(0)e^{\lambda t}$ , where  $\lambda = 4 - 4\theta - \epsilon^2 \pi^2 k^2$  is the analytic growth rate. The numerical growth rate is defined as follows:

$$\tilde{\lambda} = \frac{1}{T} \log \left( \frac{\|\phi^{N_t} - 0.5\|_\infty}{\alpha(0)} \right).$$

Let  $\phi(x, 0) = 0.5 + 0.01 \cos(k\pi x)$  be the initial profile on  $\Omega = (0, 1)$ , where  $k$  is a positive even integer of less than or equal to 20. The parameter values used in this test are  $N_x = 256$ ,  $h = 1/N_x$ ,  $\Delta t = 0.001$ ,  $N_t = 500$ ,  $\epsilon = 0.02$ ,  $\theta = 0.3$ , and  $T = 500\Delta t$ . Figure 12 shows the result of a linear stability test using our proposed method. For different wave numbers  $k$  ( $k = 0, 2, 4, \dots, 20$ ), the analytic growth rate  $\lambda$  (solid line) and numerical growth rate  $\tilde{\lambda}$  (circled markers) match each other well.

### 3.5 Spinodal decomposition of a binary mixture

In this test, we present the results of a decomposition of a binary mixture with a random initial condition. We set the initial profile on  $\Omega = (-1, 1) \times (-1, 1)$  as follows:

$$\phi(x, y, 0) = 0.5 + 0.05 \text{rand}(x, y),$$

where  $\text{rand}(x, y)$  is a random number in  $(-1, 1)$ . As the parameters, the spatial step size of  $h = 1/128$ , the temporal step size of  $\Delta t = 30h$ ,  $\epsilon = 0.025$ , and  $\theta = 0.8$  are used. Figure 13 shows the snapshots of the evolution of  $\phi(x, y, t)$  at different times, and these results are similar to those of the AC equation using the double-well polynomial potential [18]. The numerical results also indicate that the proposed scheme is stable even for a large time step.

### 3.6 Shrinking phenomenon

We confirm the shrinking phenomenon [4], which is one of the dynamics of the AC equation with the logarithm free energy potential. The parameters used are  $h = 1/128$ ,  $\Delta t = h$ , and  $\epsilon = 0.015$ . Let us consider an initial condition on  $\Omega = (-1, 1) \times (-1, 1)$  as follows:

$$\phi(x, y, 0) = \begin{cases} \phi_\beta & \text{if } |x| \leq 0.8 \text{ and } |y| \leq 0.8, \\ \phi_\alpha & \text{otherwise.} \end{cases} \tag{21}$$

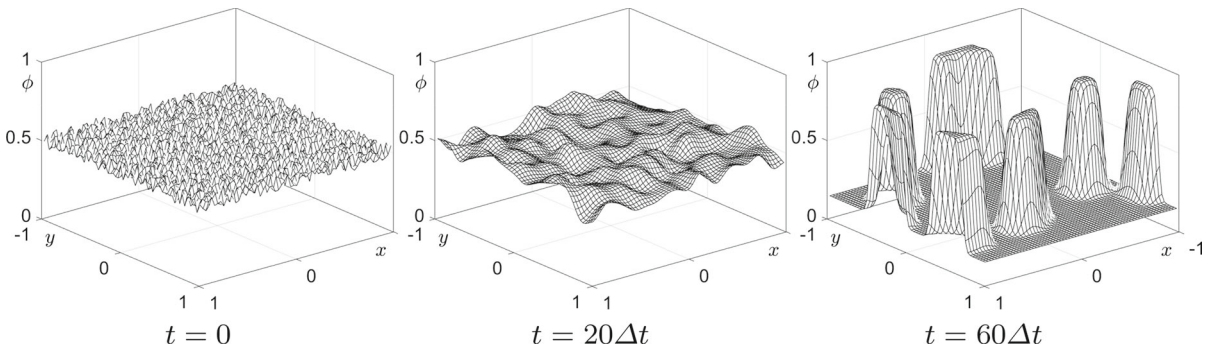
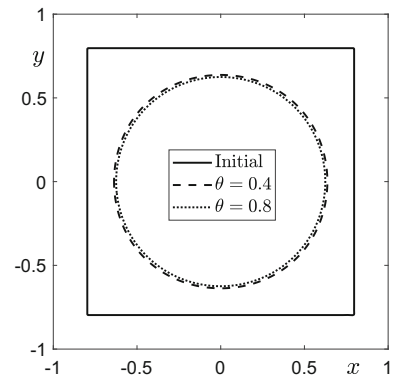


**Fig. 13** Snapshots of the evolutions of the random initial concentration  $\phi(x, y, 0)$  at different times. The initial conditions are  $\phi(x, y, 0) = 0.5 + 0.05 \text{ rand}(x, y)$ . The times are described below each figure

**Fig. 14** Shrinking phenomenon of the AC equation with logarithm free energy potential



As shown in Fig. 14, the initial square shape shrinks to a circular shape regardless of the  $\theta$  values. Here, contours are drawn at the  $\phi = 0.5$  level at  $t = 120,000\Delta t$ .

### 3.7 Decrease of the total energy

We consider the total energy decrease over time. The discrete energy  $\mathcal{E}(\phi^k)$  is defined as follows:

$$\mathcal{E}(\phi^k) = \sum_{m=1}^{N_x} \sum_{n=1}^{N_y} F(\phi_{mn}^k)h^2 + \frac{\epsilon^2}{2} \sum_{m=1}^{N_x-1} \sum_{n=1}^{N_y-1} \left[ (\phi_{m+1,n}^k - \phi_{mn}^k)^2 + (\phi_{m,n+1}^k - \phi_{mn}^k)^2 \right]. \tag{22}$$

The initial condition (21) is used. The parameter values used are  $N_x = N_y = 256$ ,  $h = 1/128$ ,  $\Delta t = h$ ,  $\epsilon = 0.015$ , and  $\theta = 0.8$ . Figure 15 shows the temporal evolution of the discrete total energy. We can confirm that the discrete total energy decreases as the number of temporal iterations increases.

### 3.8 Thickness of the interface transition layer

Next, we study the effects of  $\epsilon$  and  $\theta$  on the interface transition layer. We select four values of  $\epsilon$ , that is,  $\epsilon = 0.5h$ ,  $h$ ,  $2h$ , and  $4h$ , for each  $\theta$ . The initial condition on  $\Omega = (0, 2\pi) \times (0, \pi/4)$  is given as follows:

$$\phi(x, y, 0) = \frac{\phi_\beta - \phi_\alpha}{2} \cos(x) + \frac{\phi_\alpha + \phi_\beta}{2}, \tag{23}$$

**Fig. 15** Discrete total energy  $\mathcal{E}(\phi^k)$  over time in two-dimensional space

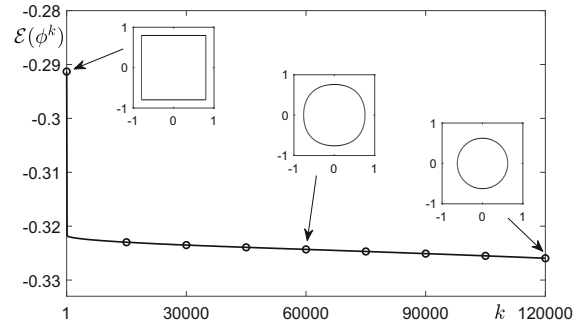


**Fig. 16** Schematic illustration of the interface layer

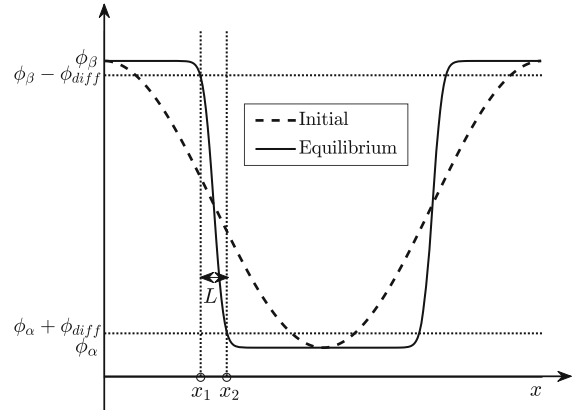


**Table 4** Thickness of the interface transition layer  $L$  with various values of  $\theta$  and  $\epsilon$

Case	$\epsilon = 0.5h$	$\epsilon = h$	$\epsilon = 2h$	$\epsilon = 4h$
$\theta = 0.3$	$0.9561h$	$2.0981h$	$4.1833h$	$7.5222h$
$\theta = 0.6$	$0.9712h$	$2.7437h$	$5.1392h$	$9.9361h$
$\theta = 0.8$	$2.2877h$	$4.3349h$	$8.3342h$	$16.4906h$
$\theta = 0.9$	$2.9795h$	$6.348h$	$12.4647h$	$24.7671h$

which means that  $\max(\phi(x, y, 0)) = \phi_\beta$  and  $\min(\phi(x, y, 0)) = \phi_\alpha$ . The parameter values  $h = 2\pi/256$  and  $\Delta t = 10h$  are used. We proceed with the evolution of the initial condition (23) until the discrete  $l_2$ -norm of the difference of two successive time step solutions is less than  $10^{-6}$ , that is,  $\|\phi^{n+1} - \phi^n\| < 10^{-6}$ . Then, we call the final state of  $\phi^{n+1}$  the equilibrium state.

Let us define the thickness of the interface transition layer  $L$  as the difference of  $x_1$  and  $x_2$ , as shown in Fig. 16. Here,  $x_1$  and  $x_2$  satisfy  $\phi(x_1, y, t) = \phi_\beta - \phi_{diff}$  and  $\phi(x_2, y, t) = \phi_\alpha + \phi_{diff}$ , respectively, where  $\phi_{diff} = (\phi_\beta - \phi_\alpha)/20$ . Table 4 shows the thickness of the interface transition layer  $L$  for the various values of  $\epsilon$  and  $\theta$ .

Furthermore, Fig. 17a and b shows the equilibrium states of  $\phi$  with  $\epsilon = 0.5h$  and  $\epsilon = 4h$ , respectively, for each  $\theta$ . The numerical result using  $\epsilon = 0.5h$  indicates the equilibrium state with a sharp interfacial transition layer, as shown in Fig. 17a. Meanwhile, the result of using  $\epsilon = 4h$  shows the relatively smooth interfacial transition layer, as shown in Fig. 17b.

By fitting the data using linear functions, we obtain the following equations:

$$\epsilon_{0.3}(L) = 0.5356L - 0.0025, \tag{24}$$

$$\epsilon_{0.6}(L) = 0.3974L + 0.0002, \tag{25}$$

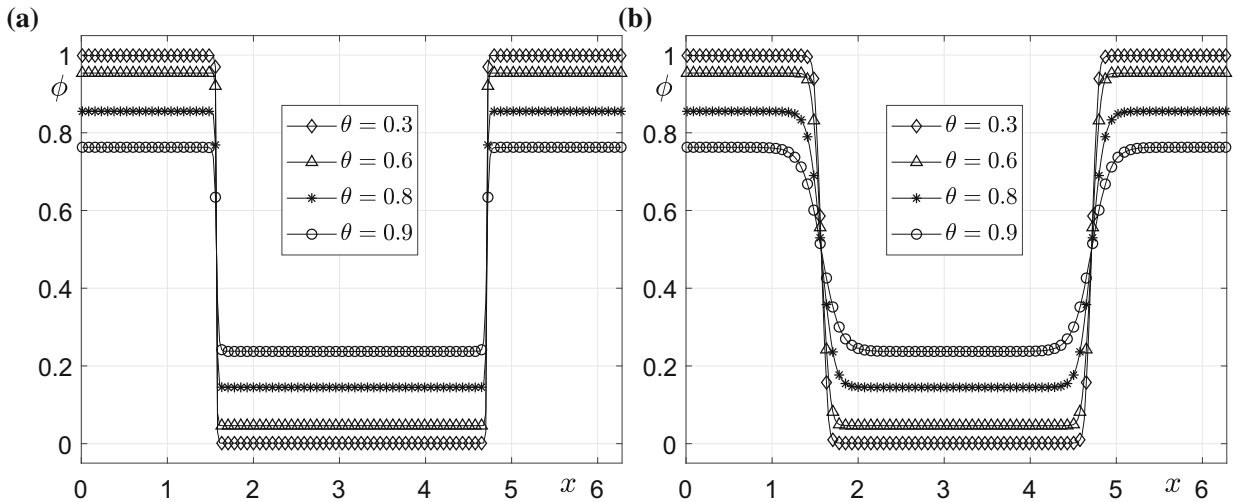
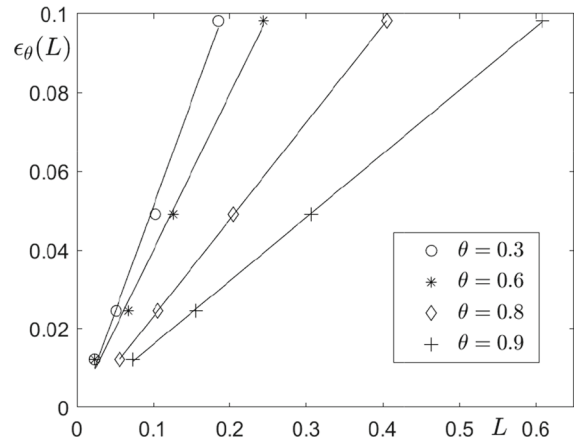


**Fig. 17** Equilibrium state for various  $\theta$  with (a)  $\epsilon = 0.5h$  and (b)  $\epsilon = 4h$

**Fig. 18**  $\epsilon_\theta(L)$  with respect to  $L$  with linear fitting functions for  $\theta = 0.3, 0.6, 0.8,$  and  $0.9$



$$\epsilon_{0.8}(L) = 0.2466L - 0.0016, \tag{26}$$

$$\epsilon_{0.9}(L) = 0.1614L - 0.0001. \tag{27}$$

Figure 18 shows  $\epsilon_\theta(L)$  with respect to  $L$  with linear fitting functions for  $\theta = 0.3, 0.6, 0.8,$  and  $0.9$ .

### 3.9 Motion by mean curvature

Let us consider the following rescaled AC equation:

$$\frac{\partial \phi(\mathbf{x}, t)}{\partial t} = -\frac{F'(\phi(\mathbf{x}, t))}{\epsilon^2} + \Delta \phi(\mathbf{x}, t), \quad \mathbf{x} \in \Omega, \quad t > 0. \tag{28}$$

Motion by mean curvature is an important feature of the AC equation. The radius at time  $t$  is  $R(t) = \sqrt{R_0^2 + 2(1-d)t}$ , where  $R_0$  is the initial radius. Please refer to [19] for further details. Here, we conduct a two-dimensional test using the following initial condition:

$$\phi(x, y, 0) = \frac{\phi_\beta - \phi_\alpha}{2} \tanh\left(\frac{1 - \sqrt{x^2 + y^2}}{2\sqrt{2}\epsilon}\right) + \frac{\phi_\alpha + \phi_\beta}{2} \tag{29}$$

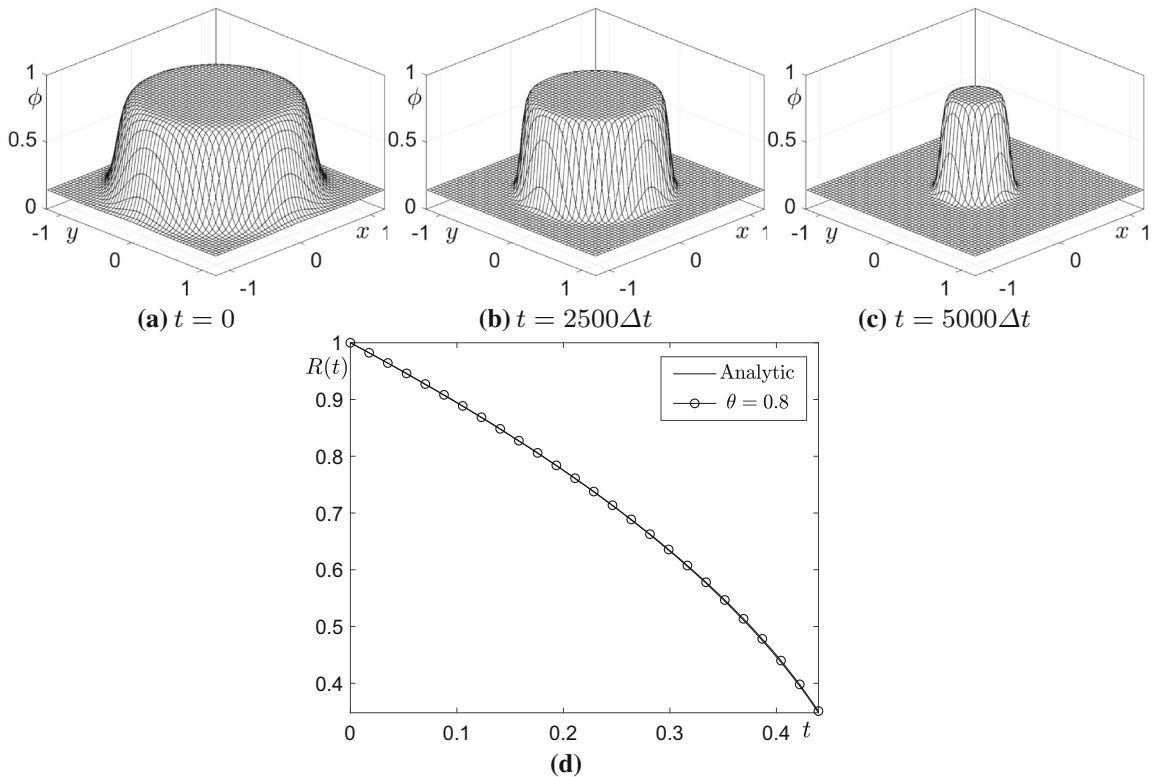


**Fig. 19** a–c Evolutions of the initial concentration  $\phi(x, y, 0)$  with  $\theta = 0.8$  at different times, as described below each figure. **d** Analytic and numerical solutions to the evolution of the radius with  $\theta = 0.8$

on the computational domain  $(-1.2, 1.2) \times (-1.2, 1.2)$  with  $N_x = N_y = 256$ . The parameters used are  $h = 2.4/256$ ,  $\theta = 0.8$ , and  $\Delta t = h^2$ . In particular, we use  $\epsilon = \epsilon_{0.8}(14h)$  from Eq. (26), that is,  $L = 14h$ . Figure 19a–c shows the snapshots of  $\phi$  at different times. As shown in Fig. 19d, the radius of the circle shrinks over time and is similar to an analytic solution. This result indicates that the motion by mean curvature is well preserved in the AC equation with the logarithm potential energy.

### 3.10 Three-dimensional case

The governing equation (5) and the proposed numerical method can be straightforwardly applied to three-dimensional domain. First, the spinodal decomposition test is conducted in three-dimensional domain  $\Omega = (-1, 1) \times (-1, 1) \times (-1, 1)$ . A random initial condition is given as follows:

$$\phi(x, y, z, 0) = 0.5 + 0.3 \text{rand}(x, y, z), \tag{30}$$

where  $\text{rand}(x, y, z)$  is a random number in  $(-1, 1)$ . For a three-dimensional case, the parameters used are  $N_x = N_y = N_z = 64$ ,  $h = 1/32$ ,  $\Delta t = 30h$ ,  $\epsilon = 0.025$ , and  $\theta = 0.8$ . Figure 20 shows the snapshots of the evolution of  $\phi(x, y, z, t)$  at different times. On a three-dimensional case, even with a large time step, stable results are obtained. The results are similar to the dynamics of the AC equation using the double-well polynomial potential [18].

Next, we consider the dynamics of the motion by mean curvature on a three-dimensional case. The initial condition and the parameters used in this test are as follows:

$$\phi(x, y, z, 0) = \frac{\phi_\beta - \phi_\alpha}{2} \tanh\left(\frac{1 - \sqrt{x^2 + y^2 + z^2}}{2\sqrt{2}\epsilon}\right) + \frac{\phi_\alpha + \phi_\beta}{2} \tag{31}$$

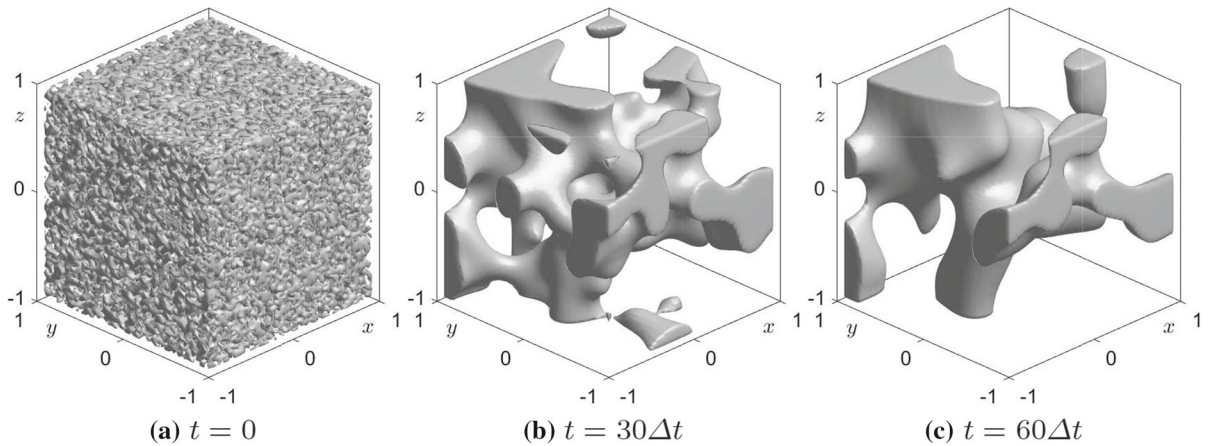


**Fig. 20** Snapshots of evolutions of the random initial concentration  $\phi(x, y, z, 0)$  at different times. The initial conditions are  $\phi(x, y, z, 0) = 0.5 + 0.3 \text{ rand}(x, y, z)$ . The times are described below each figure

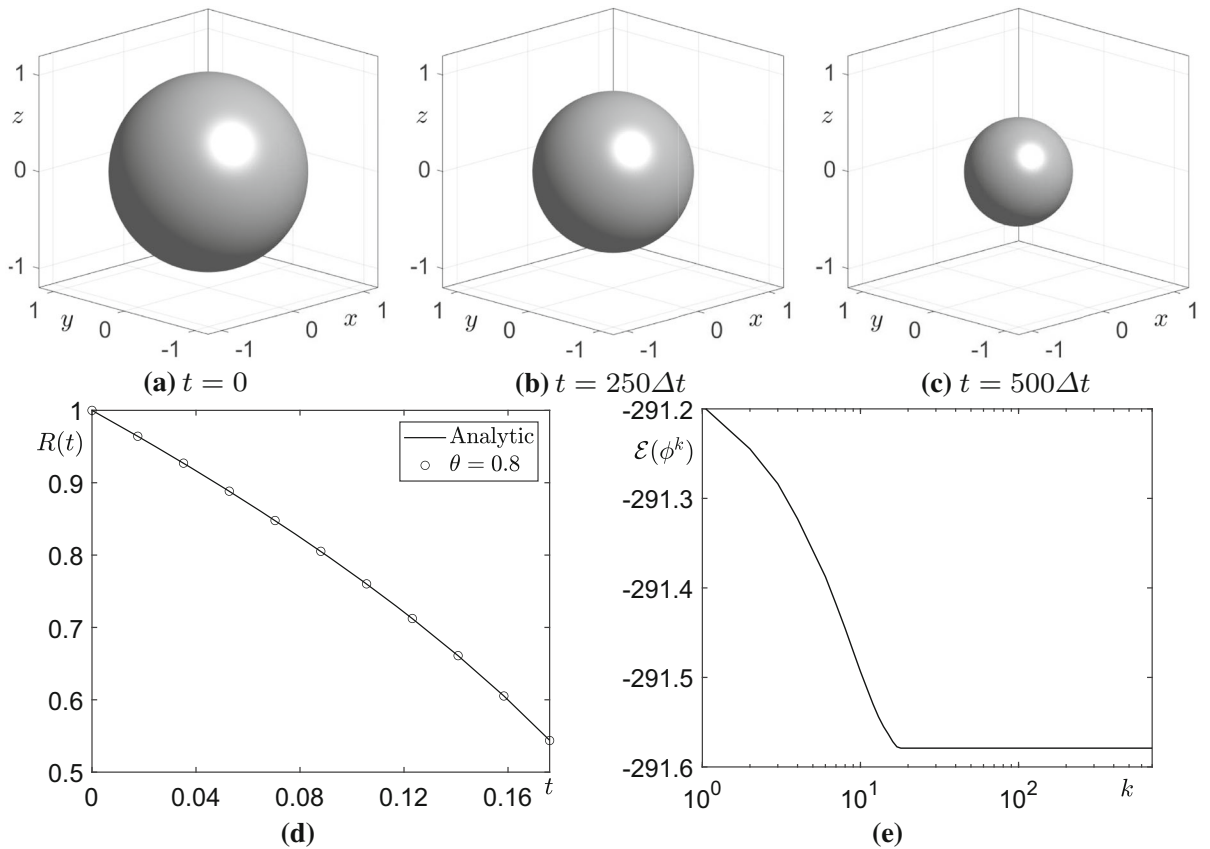


**Fig. 21** a–c Evolutions of the initial concentration  $\phi(x, y, z, 0)$  with  $\theta = 0.8$  at different times as described below each figure. d Analytic and numerical solutions of the evolution of the radius with  $\theta = 0.8$ . e Discrete total energy  $\mathcal{E}(\phi^k)$  over time in three-dimensional space



on the computational domain  $(-1.2, 1.2) \times (-1.2, 1.2) \times (-1.2, 1.2)$  with  $N_x = N_y = N_z = 128$ ,  $h = 2.4/128$ ,  $\theta = 0.8$ ,  $\epsilon = \epsilon_{0.8}(14h)$ , and  $\Delta t = h^2$ . We also define the 3D discrete energy  $\mathcal{E}(\phi^k)$  as

$$\begin{aligned} \mathcal{E}(\phi^k) &= \sum_{m=1}^{N_x} \sum_{n=1}^{N_y} \sum_{l=1}^{N_z} F(\phi_{mnl}^k) \frac{h^3}{\epsilon^2} \\ &+ \frac{h}{2} \sum_{m=1}^{N_x-1} \sum_{n=1}^{N_y-1} \sum_{l=1}^{N_z-1} \left[ (\phi_{m+1,nl}^k - \phi_{mnl}^k)^2 + (\phi_{m,n+1,l}^k - \phi_{mnl}^k)^2 + (\phi_{mn,l+1}^k - \phi_{mnl}^k)^2 \right]. \end{aligned}$$

Figure 21a–c shows the snapshots of  $\phi$  at a level of 0.5. The decrease in radius is compared to the analytic solution over time. Figure 21e shows the discrete total energy for the initial condition (31). As with the two-dimensional test, the result confirms that the analytic and numerical solutions are in good agreement.

## 4 Conclusions

In this paper, we developed an unconditionally stable numerical method for the AC equation with logarithmic free energy. The logarithmic energy is more physically meaningful than the commonly used fourth-order polynomial potentials. However, owing to the singularity of the logarithmic free energy, it is difficult to develop unconditionally stable numerical methods for the AC equation with the logarithmic free energy. To overcome this difficulty, previous methods involved adding a stabilizing term to the logarithmic energy or using a regularized potential. By contrast, we used an interpolation method that does not add a stabilizing term nor regularize the logarithmic energy. Various numerical experiments were conducted to demonstrate the performance of the proposed method. The proposed solution algorithm may be a useful tool in a study on the dynamics of the AC equation with the logarithmic free energy. Compared to convex–concave splitting techniques, we do not introduce a stabilizing parameter that may cause time step rescaling [20]. Herein, we used the finite difference method, which is simple and easy to combine with other settings such as the Navier–Stokes equation. However, the proposed scheme can also be applied to other frameworks such as the finite element method [21, 22], which is a good approach to solving equations on complex domains.

**Acknowledgements** C. Lee was supported by the National Research Foundation(NRF), Korea, under project BK21 FOUR. Y. Choi was supported by National Research Foundation of Korea (NRF) grant funded by the Korea Government (NRF-2020R1C1C1A0101153712). The corresponding author (J.S. Kim) was supported by Basic Science Research Program through the National Research Foundation of Korea (NRF) funded by the Ministry of Education(NRF-2019R1A2C1003053). The authors are grateful to the reviewers whose valuable suggestions and comments significantly improved the quality of this article.

## References

- Allen SM, Cahn JW (1979) A microscopic theory for antiphase boundary motion and its application to antiphase domain coarsening. *Acta Metall* 27:1085–1095
- Kornhuber R, Krause R (2006) Robust multigrid methods for vector-valued Allen–Cahn equations with logarithmic free energy. *Comput Vis Sci* 9(2):103–116
- Lee D, Huh JY, Jeong D, Shin J, Yun A, Kim J (2014) Physical, mathematical, and numerical derivations of the Cahn–Hilliard equation. *Comput Mater Sci* 81:216–225
- Wang X, Kou J, Cai J (2020) Stabilized energy factorization approach for Allen–Cahn equation with logarithmic Flory–Huggins potential. *J Sci Comput* 82(2):25
- Jeong D, Lee S, Kim J (2015) An efficient numerical method for evolving microstructures with strong elastic inhomogeneity. *Model Simul Mater Sci Eng* 23(4):045007
- Shen J, Tang T, Yang J (2016) On the maximum principle preserving schemes for the generalized Allen–Cahn equation. *Commun Math Sci* 14(6):1517–1534
- Bartels S, Müller R (2011) Error control for the approximation of Allen–Cahn and Cahn–Hilliard equations with a logarithmic potential. *Numer Math* 119(3):409–435

8. Chen W, Wang C, Wang X, Wise SM (2019) Positivity-preserving, energy stable numerical schemes for the Cahn–Hilliard equation with logarithmic potential. *J Comput Phys* 3:100031
9. Lee C, Kim H, Yoon S, Kim S, Lee D, Park J, Kwak S, Yang J, Wang J, Kim J (2021) An unconditionally stable scheme for the Allen–Cahn equation with high-order polynomial free energy. *Commun Nonlinear Sci Numer Simul* 95:105658
10. Lee HG, Shin J, Lee JY (2015) First and second order operator splitting methods for the phase field crystal equation. *J Comput Phys* 299:82–91
11. Lee HG (2017) A semi-analytical Fourier spectral method for the Swift–Hohenberg equation. *Comput Math Appl* 74(8):1885–1896
12. Holden H, Karlsen KH, Risebro NH, Tao T (2011) Operator splitting for the KdV equation. *Math Comput* 80(274):821–846
13. Tinoco-Guerrero G, Domínguez-Mota FJ, Tinoco-Ruiz JG (2020) A study of the stability for a generalized finite-difference scheme applied to the advection-diffusion equation. *Math Comput Simul* 176:301–311
14. Choi Y, Jeong D, Lee S, Kim J (2015) Numerical implementation of the two-dimensional incompressible Navier–Stokes equation. *J KSIAM* 19:103–121
15. Burden RL, Faires JD (2005) *Numerical Analysis*, 8th edn. Thomson Brooks/Cole, Stamford
16. Hamiaz A, Ferrieres X, Pascal O (2020) Efficient numerical algorithm to simulate a 3D coupled Maxwell-plasma problem. *Math Comput Simul* 174:19–31
17. Thomas JW (1995) *Numerical partial differential equations: finite difference methods*. Springer, New York
18. Li Y, Jeong D, Kim H, Lee C, Kim J (2019) Comparison study on the different dynamics between the Allen–Cahn and the Cahn–Hilliard equations. *Comput Math Appl* 77(2):311–322
19. Li Y, Lee HG, Jeong D, Kim J (2010) An unconditionally stable hybrid numerical method for solving the Allen–Cahn equation. *Comput Math with Appl* 60(6):1591–1606
20. Lee S, Kim J (2019) Effective time step analysis of a nonlinear convex splitting scheme for the Cahn–Hilliard equation. *Commun Comput Phys* 25:448–460
21. Copetti MIM, Elliott CM (1992) Numerical analysis of the Cahn–Hilliard equation with a logarithmic free energy. *Numer Math* 63(1):39–65
22. Garcke H, Lam KF, Styles V (2018) Cahn–Hilliard inpainting with the double obstacle potential. *SIAM J Imaging Sci* 11(3):2064–2089

**Publisher’s Note** Springer Nature remains neutral with regard to jurisdictional claims in published maps and institutional affiliations.